



HAL
open science

Performance of four digital algorithms for γ - γ timing with LaBr₃(Ce) scintillators

G. Simpson, S. Curtoni, D. Dauvergne, M.-L. Gallin-Martel, S. Marcatilli, G.
Thiamova

► **To cite this version:**

G. Simpson, S. Curtoni, D. Dauvergne, M.-L. Gallin-Martel, S. Marcatilli, et al.. Performance of four digital algorithms for γ - γ timing with LaBr₃(Ce) scintillators. Nuclear Instruments and Methods in Physics Research Section A: Accelerators, Spectrometers, Detectors and Associated Equipment, 2019, 40, pp.50-55. 10.1016/j.nima.2019.05.015 . hal-02134630

HAL Id: hal-02134630

<https://hal.science/hal-02134630>

Submitted on 25 Oct 2021

HAL is a multi-disciplinary open access archive for the deposit and dissemination of scientific research documents, whether they are published or not. The documents may come from teaching and research institutions in France or abroad, or from public or private research centers.

L'archive ouverte pluridisciplinaire **HAL**, est destinée au dépôt et à la diffusion de documents scientifiques de niveau recherche, publiés ou non, émanant des établissements d'enseignement et de recherche français ou étrangers, des laboratoires publics ou privés.



Distributed under a Creative Commons Attribution - NonCommercial 4.0 International License

1 Performance of Four Digital Algorithms for $\gamma - \gamma$
2 Timing with LaBr₃(Ce) Scintillators

3 G. Simpson, S. Curtoni, D. Dauvergne, M.-L. Gallin-Martel, S. Marcatilli,
4 G. Thiamova

5 *LPSC, Université Grenoble Alpes, CNRS/IN2P3, Institut National Polytechnique de*
6 *Grenoble, F-38026 Grenoble Cedex, France*

7 **Abstract**

8 Time resolution measurements were performed using four digital timing
9 algorithms and a pair of truncated-cone shaped, 38-mm diameter LaBr₃(Ce)
10 fast-timing scintillator detectors. The best resolution [FWHM=143(3) ps] was
11 found for transitions from a ⁶⁰Co source when fitting the rising part of sampled
12 waveforms with a cubic polynomial and applying a leading-edge threshold. An
13 average-pulse autocovariance function performed slightly worse [155(3) ps], but
14 was found to be better than digital constant-fraction [178(4) ps] and leading-
15 edge [177(4) ps] algorithms. Use of a ¹⁵²Eu source allowed the performance
16 of the four algorithms to be tested across a range of γ -ray energies with the
17 LaBr₃(Ce) detectors. Here the autocovariance algorithm performed best. Chang-
18 ing the sampling speed showed minimal degradation in the time resolution at
19 20 GS/s, though at 4 GS/s the resolutions were 30–60 % worse. These results
20 show that at sampling speeds of 20 or 40 GS/s the time resolutions obtained are
21 close to those reported for analogue pulse-processing electronics. Compared to
22 other works, using slower sampling speeds but higher vertical resolution, slightly
23 worse performance was obtained.

24 **1. Introduction**

25 Fast scintillator detectors are used for $\gamma - \gamma$ timing and have a wide range
26 of applications, including lifetime measurements of excited nuclear states [1],

27 medical positron-emission tomography (PET) and range monitoring in hadron
28 therapy [2]. These scintillation crystals have the properties of modest energy
29 resolution and fast decay times (ns), and are constructed often with the aim
30 of optimising the time rather than energy resolution of the system. Recent
31 progress in the fabrication of lanthanide-halide crystals, such as $\text{LaBr}_3(\text{Ce})$, with
32 an energy resolution of $\sim 3\%$ at 662 keV and time resolution as good as 98(2) ps
33 for ~ 1.2 MeV photons [3] has given renewed interest in the use and development
34 scintillator detectors, resulting in, for example, the construction of the FATIMA
35 array [4, 5]. The decay time of $\text{LaBr}_3(\text{Ce})$ is 16 ns and 63000 photons are emitted
36 per MeV of energy absorbed. This compares with a decay time of 0.7 ns and
37 1800 photons/MeV for the fast component of the commonly used BaF_2 . These
38 scintillator detectors can be used to measure nuclear-state lifetimes in the 10s-
39 of-ps-to-ns time range [1, 6, 7]. To date analogue signal processing chains have
40 been almost exclusively used in applications which require the very best time
41 resolution.

42 In principle digital acquisition systems, with very high-speed sampling, should
43 allow equivalent, or even improved, timing performance over analogue ones, as
44 signal processing can reduce jitter and fixed-frequency noise and bespoke al-
45 gorithms can be developed for a particular detection system. Recently, time
46 resolutions approaching, and matching, the best ones achieved with analogue
47 electronics have been obtained with $\text{LaBr}_3(\text{Ce})$ detectors, using digitizers with
48 sampling frequencies of 0.5, 4 and 5 GS/s by applying digital timing algorithms
49 [8–10]. An improved time resolution over analogue systems was earlier obtained
50 with Ge detectors using digital pulse-shape analysis [11]. Furthermore, digital
51 acquisition systems have other advantages over analogue ones including (poten-
52 tially) lower cost per channel, fewer modules and timing stamping of individual
53 hits, allowing offline event reconstruction. Any algorithms used for pulse-shape
54 analysis should ideally be simple and efficient enough to be implemented on field-
55 programmable gate arrays (FPGAs), allowing real-time processing. Pulse-shape
56 analysis has already been used to perform, for example, α/γ discrimination in
57 $\text{LaBr}_3(\text{Ce})$ crystals [12] and neutron/ γ selection in liquid scintillators [13].

58 The purely statistical resolving time of a pair of detectors is given by $\delta t = \frac{\sigma}{\sqrt{n}}$
59 where n is the number of events and σ is the width parameter of the Gaussian
60 function describing the distribution. Hence an experiment using detectors with
61 twice worse time resolution will require 4 times the number of counts to achieve
62 the same statistical precision. Therefore there is strong motivation to develop
63 timing algorithms suitable for use with digital acquisition systems which have
64 performances equivalent to, or better than, the best analogue pulse-processing
65 electronics.

66 Improved timing resolution is also of interest for clinical PET applications,
67 which would allow lower injected patient doses. Although the γ -ray detectors
68 used in PET applications are much smaller than the crystals used for nuclear
69 excited-state lifetime measurements, equivalent pulse-processing techniques are
70 used to extract timing information. Clinical PET time resolutions better than
71 100 ps would allow some of the artefacts affecting tomographic reconstruction
72 to be removed for devices with partial angular coverage [14]. For resolutions of
73 10 ps time-consuming image reconstruction techniques would not be required,
74 as true real-time 3-D image information would be available [14]. In the case of
75 prompt- γ timing for particle therapy, transitions with energies typically in the
76 range 3–6 MeV are measured, for which better time resolution is expected than
77 at 511 keV [2].

78 With this in mind we have measured the time resolution of a pair of fast
79 LaBr₃(Ce) scintillator detectors when applying four different algorithms to ex-
80 tract timing information. These algorithms were a leading-edge discrimination
81 of the raw detector pulse and also following a cubic polynomial fit to the rising
82 slope, a digital constant-fraction discriminator and an ideal-pulse autocovari-
83 ance function. The first and third pulse-processing algorithms are equivalent to
84 analogue fast-signal treatment schemes. These algorithms differ from other fast
85 filters often implemented on commercial digital acquisitions systems for use with
86 Ge detectors, such as trapezoidal ones. These fast-filters have the aim of distin-
87 guishing real low-energy signals from noise. Limited tests of these algorithms
88 within the present work gave degraded timing performance in comparison with

89 the ones used below, however this does not exclude that a well-tuned algorithm
90 of this type, with its inherent noise filtering, may give improved results in the
91 future. The experiments were performed with a digital oscilloscope running at
92 a sampling frequency of 40 GS/s, with a 4 GHz bandwidth and 10-bit vertical
93 resolution. The effect of varying the sampling frequency was also studied.

94 **2. Experimental Setup**

95 The time resolution of $\gamma - \gamma$ coincidences detected in a pair of scintillator
96 detectors was studied in order to determine pulse-processing algorithm perfor-
97 mance. A pair of truncated-cone shaped $\text{LaBr}_3(\text{Ce})$ scintillator detectors were
98 used to detect γ rays emitted from ^{60}Co and ^{152}Eu radioactive sources. The
99 detectors were placed ~ 2.5 cm from the source and at 90° to each other, to
100 minimise Compton scattering. The $\text{LaBr}_3(\text{Ce})$ crystals were 38 mm long and
101 38-mm wide at the base. Their exact dimensions are reported in [3]. These crys-
102 tals were mounted on Hamamatsu R9779 photomultiplier tubes (PMTs). The
103 anode output signal of the PMT base was connected directly to the oscilloscope
104 and the dynode output was terminated with a $50\text{-}\Omega$ resistor. The oscilloscope
105 was a LeCroy HDO9404 model with 10-bit vertical resolution and a vertical
106 range of 1 V. It ran at a sampling speed of 40 GS/s. Each digitized trace was
107 4096 samples (102.4 ns) long, enough to contain all of the $\text{LaBr}_3(\text{Ce})$ signal
108 trace. The oscilloscope ran in an “AND” mode where traces were captured only
109 if triggers on both signals fired within a time window of a few nanoseconds. The
110 high voltage was set to ~ -1100 V so that pulses with energies up to ~ 1.5 MeV
111 could be recorded on the oscilloscope. This voltage is slightly lower than the
112 -1200 V used in [3], which was found to be optimal with the same detectors.
113 The limited vertical acceptance range of the oscilloscope (1 V) meant that the
114 optimal voltage could not be used. However, in [15] the difference in resolution
115 between $\text{LaBr}_3(\text{Ce})$ detectors operating at -1100 V and -1300 V was found to
116 be ~ 15 ps. Hence the use of a slightly lower than optimal voltage is expected
117 to result in only a small degradation in time resolution (< 15 ps).

118 Data taken with a 264-kBq ^{60}Co source were used to find the best resolution
119 of each algorithm at energies of ~ 1.2 MeV. This source first β^- decays and then
120 emits a cascade of two γ rays of energy 1173.2- and 1332.5-keV. The half-life of
121 the intermediate state is 0.7 ps, negligible compared to the time resolution of
122 the γ -ray detectors. Some 3×10^5 coincident traces were captured.

123 A 27.0-kBq ^{152}Eu source was used to determine how the different algorithms
124 perform for γ -ray transitions across a wider energy range. A total of $3.1 \times$
125 10^6 coincidence traces were recorded. Around 20 intense γ rays are emitted
126 by this source, which form $\gamma - \gamma$ cascades distributed in two nuclei, ^{152}Gd
127 and ^{152}Sm [16]. These cover an energy range of 121.8 to 1299.1 keV, however
128 several lifetimes of the intermediate states are in the 100-ps-to-ns time range.
129 Use of these cascades would add appreciable widths to time spectra and are
130 unsuitable for this study. However the 344.3-keV transition is coincident with
131 five transitions covering an energy range of 367.8–1299.1 keV. For four of these
132 $\gamma - \gamma$ coincidences the intermediate state is the 344.3-keV one, with a lifetime
133 of 46.7 ps [16]. The fifth one is the 367.8–344.3-keV coincidence which is part
134 of a triple- γ cascade with a mean lifetime of 57.2 ps. Therefore for this set
135 of $\gamma - \gamma$ cascades mean lifetimes of a similar ~ 50 ps are present, allowing a
136 qualitative comparison of the performance of each algorithm as a function of
137 the γ -ray energy coincident with a 344.3-keV transition. The performance of
138 these algorithms at energies of around 511 keV is relevant to PET applications
139 [17], though the crystals used in the current study are optimised for lifetime
140 measurements of excited nuclear states.

141 3. Algorithms and Results with ^{60}Co

142 Before applying any timing algorithms the first procedure was to extract the
143 average value of the pulse baseline. This quantity varies from pulse to pulse and
144 was obtained simply by finding the average of the first 300 sample points. These
145 all lie at times earlier than the first sample point registering the interaction of a
146 γ ray, as can be seen in Fig. 1. This shows a typical anode pulse from one of the
147 $\text{LaBr}_3(\text{Ce})$ detectors captured by the oscilloscope. The data points presented

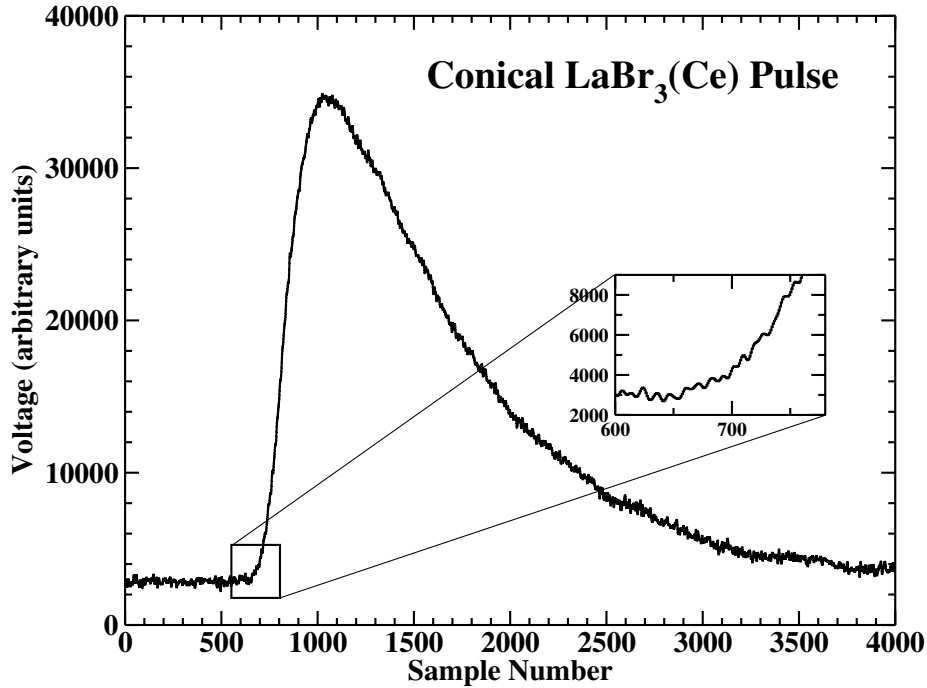


Figure 1: Example of an anode pulse captured by the 40 GS/s oscilloscope. The data points shown are the ones analysed and these are the raw ones reflected about the x -axis, as explained in the text. The zoomed inset allows the noise present in the baseline and at the start of the rising pulse to be observed.

148 were reflected across the x -axis so that all values are positive. This was done
 149 to simplify algorithm implementation. The energy of the deposited γ -ray signal
 150 was found using a simple running integration algorithm, which sums all sample
 151 points found above the baseline. An energy resolution (FWHM) of 3.4(1) %
 152 was measured at 1332.5 keV, the same as reported in [9, 10].

153 If the energies of both pulses were found to fall within ± 20 keV of the
 154 individual photopeak energies of interest then timing algorithms were applied
 155 to the event. These algorithms are listed below. Examples of gated energy
 156 spectra measured using the ^{60}Co source are shown in Fig. 2. Here one observes
 157 only the other transition of the $\gamma - \gamma$ cascade and Compton background.

158 In order to quantify the timing performance of each algorithm when analysing
 159 $\gamma - \gamma$ events, differences between the trigger times of each detector were plot-

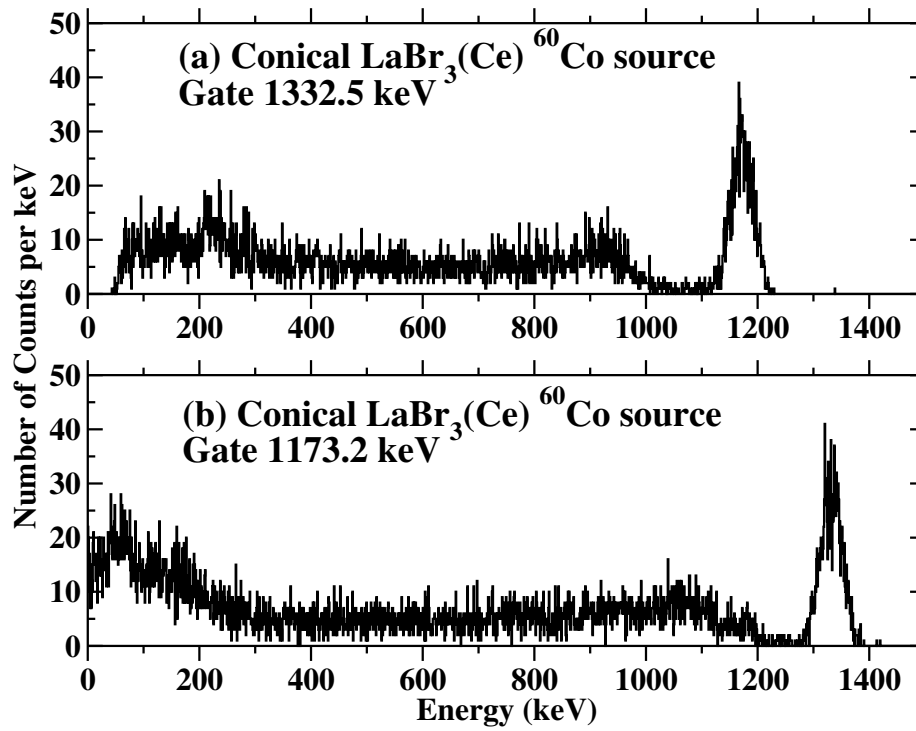


Figure 2: Energy spectra obtained with the $\text{LaBr}_3(\text{Ce})$ detectors when energy gates are set on one transition and then the other of the cascade.

160 ted. In all cases the full-width half-maximum (FWHM) value of the assumed
161 Gaussian time distribution is used to define the resolution. As the detectors are
162 essentially identical, then the measured FWHM can be divided by $\sqrt{2}$ to obtain
163 the resolution of each individual detector, to a good approximation. This allows
164 a comparison with results reported in the literature for each detector type, for
165 example those of [3]. Identical γ -ray gates were set when processing the data
166 with each algorithm.

167 *3.1. Leading edge with a ^{60}Co source*

168 The leading-edge algorithm produces a trigger-time marker when the pulse
169 trace first crosses a set threshold. For the data taken with the ^{60}Co source, the
170 FWHM was measured as a function of the threshold energy. Use of interpolation
171 between the sample points did not improve the time resolution. This agrees with
172 the conclusions of [8] for high sampling frequencies. There it was reasoned that
173 the higher density of sampling points means that the difference between the
174 actual detector pulse and a linear interpolation between any two sample points
175 becomes negligible.

176 An example time spectrum obtained with the $\text{LaBr}_3(\text{Ce})$ detectors is shown
177 in Fig. 3. The results obtained are shown in Fig. 4 where the change in FWHM
178 is shown as a function of the threshold value. The maximum pulse height is
179 around 35000 (arbitrary units) and the best FWHM values are obtained with
180 the threshold set at 10–20 % of this maximum. A similar behaviour is found
181 in analogue leading-edge modules and in previous studies using digital leading-
182 edge algorithms (15 %) [17]. One observes that there is a regular degradation
183 of the FWHM with increasing threshold values. Threshold values below ~ 5 %
184 of the pulse height produced spurious peaks due to noise. The best resolution
185 obtained with this algorithm was 177(4) ps.

186 *3.2. Cubic Polynomial Slope Fit and Leading Edge with a ^{60}Co source*

187 In order to remove any high-frequency noise contribution to the leading-edge
188 algorithm, the rising slope of each trace was captured and fitted with a cubic
189 polynomial function. This function was the lowest order polynomial found to

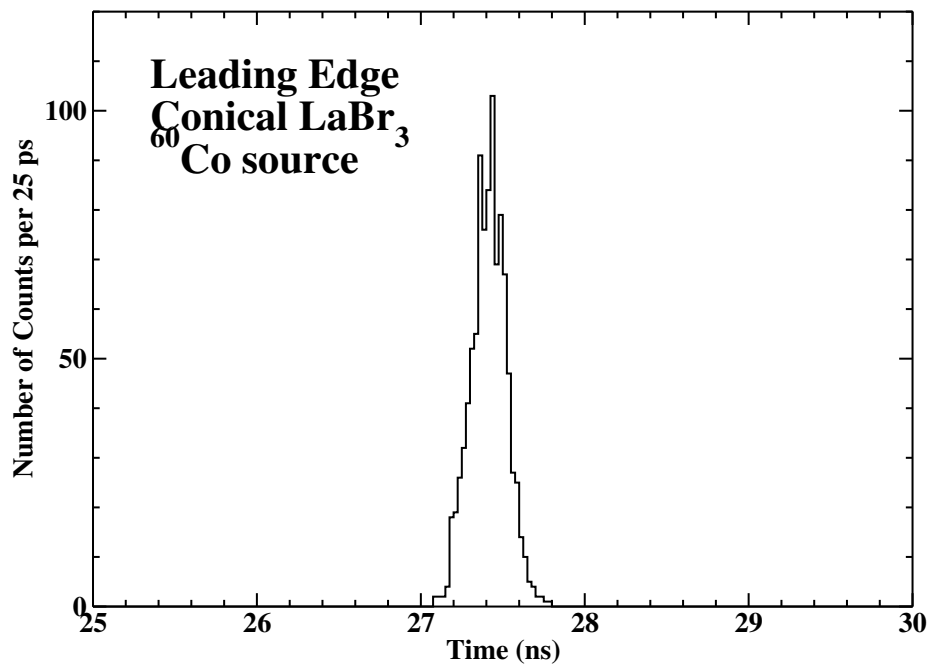


Figure 3: Example time spectrum measured with the leading edge algorithm and a ⁶⁰Co source.

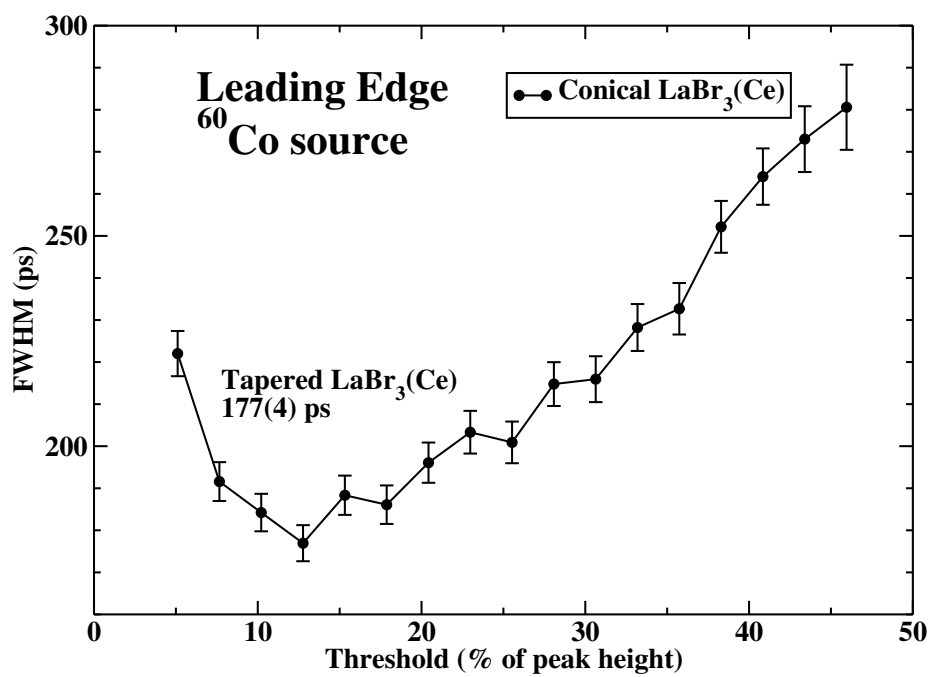


Figure 4: Full width half maximum (FWHM) of time signals obtained with a leading-edge algorithm as a function of the threshold value for a single detector, de-convoluted from the measured distribution.

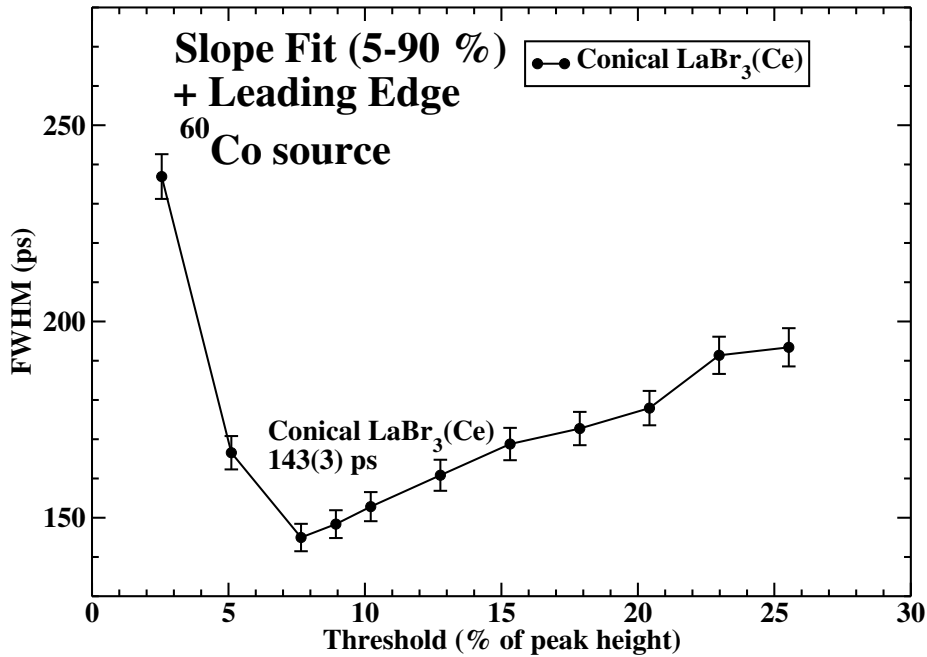


Figure 5: Full width half maximum (FWHM) of time signals obtained with a cubic slope-fit algorithm as a function of the threshold value for a single detector, de-convoluted from the measured distribution.

190 accurately reproduce the rising edge of the detector pulses, in line with the
 191 results of [18]. A leading edge threshold was then applied to the fit function
 192 describing each individual pulse, producing a reference time. Fits were applied
 193 across rising slopes varying from 10 %–90 %, 5 %–90 %, 5 %–50 % and 5 %–30 %
 194 of the pulse peak height. The best results were obtained for fits over the range
 195 5 %–90 % and 5 %–50 % of pulse height, where equivalent time resolutions,
 196 within errors [143(3) ps], were obtained. The threshold parameter was also
 197 varied until the smallest FWHM was found. A value close to the one in Sec. 3.1
 198 was optimal. The results are shown in Fig. 5. One notes that it is possible to
 199 apply this algorithm with a lower threshold value than for the raw signals of
 200 Sec. 3.1, due to the absence of high-frequency noise on the fitted polynomial
 201 function.

202 The digital leading-edge algorithm of Sec. 3.1 and the cubic polynomial slope
 203 fit, followed by a leading edge trigger, used here trigger on signals in a very sim-

204 ilar manner. A comparison of the results obtained by each allows an estimation
 205 of the influence of higher frequency noise harmonics on the signal time resolu-
 206 tion, because high-frequency noise is smoothed out in the fit analysis. As noise
 207 contributions add in quadrature, then one obtains $\text{FWHM}_{\text{highfreq}}=104(3)$ ps
 208 for the high-frequency noise component, a significant amount.

209 3.3. Constant Fraction with a ^{60}Co source

210 The constant fraction (CFD) algorithm used in the analysis of the detector
 211 signals is the digital equivalent of the ones used in analogue modules. An input
 212 signal is duplicated, inverted and delayed. The original signal is then attenuated
 213 by a fraction f and the zero-crossing of the sum of these two signals corresponds
 214 to the reference time. The CFD algorithm is written as

$$\text{CFD}[i] = f \times V[i] - V[i - \text{delay}] \quad (1)$$

215 where f is the fraction of the attenuated signal, $V[i]$ is the pulse height of the
 216 sample at bin number i and delay is the time by which the duplicated signal is
 217 retarded [19]. This algorithm was tested over a range of values of f , from ~ 0.2
 218 to 0.4, corresponding to the ones used in analogue modules. Values of f below
 219 0.15 could not be applied due to noise. The results are shown in Fig. 6. Similarly
 220 the delay parameter was varied until an optimal result was obtained. The best
 221 delay values are close to the peak rise time, again in line with the settings of
 222 an analogue CFD. The performance of the algorithm is relatively insensitive to
 223 changes in delay times over a large range of values, as shown in Fig. 7. A time
 224 resolution of 178(4) ps was the best one obtained with this algorithm.

225 3.4. Autocovariance with averaged pulse-shapes with a ^{60}Co source

226 For each pair of applied energy gates pulses in each detector were summed
 227 and then averaged. This produced approximately “ideal” pulses, almost noise
 228 free, though still retaining any subtle systematic inflexions inherent to each
 229 detector pulse.

230 Once the set of average pulses had been obtained then each pulse in a given
 231 detector, falling within the range of the energy gate, was then compared to it.

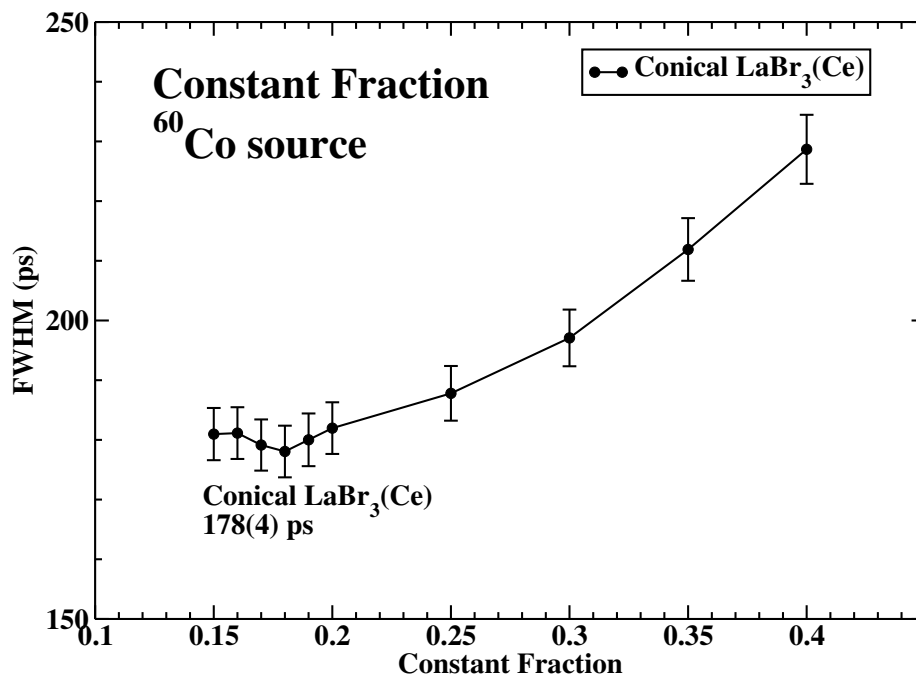


Figure 6: Full width half maximum (FWHM) of a digital constant-fraction algorithm as a function of the fraction of the attenuated signal for a single detector, de-convoluted from the measured distribution. A delay of 6.25 ns was used.

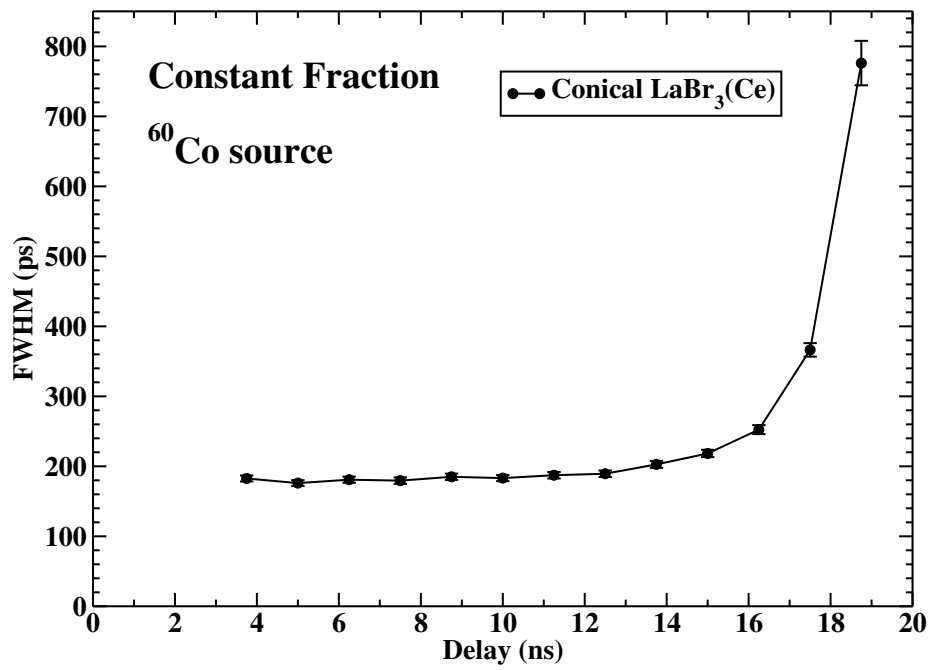


Figure 7: Full width half maximum (FWHM) of a digital constant-fraction algorithm as a function of the delay time of the duplicated signal for a single detector, de-convoluted from the measured distribution. A fraction of $f=0.18$ was used.

232 This was done by calculating the variance between the rising slope of a pulse
233 of a given event and the average one, within the same height interval, using
234 Welford’s algorithm [20]. The event pulse was then shifted by one sample and
235 the variance calculated again. Once the variance had been calculated across
236 a set range of shifts, the minimum variance was obtained, allowing the “lag”
237 between the individual pulse and the average one to be determined. The lag
238 value can then be used to determine a trigger time. It is worth noting that this
239 algorithm has no threshold dependence.

240 The vertical range over which the variance was calculated was changed and
241 the optimal one was found to be 5–20 % of the pulse height, giving a resolution
242 of 155(3) ps. This is shown in Fig. 8, where resolution is plotted as a function
243 of analysed pulse height. Equivalent results were obtained when comparing 20
244 channels of the event pulse to the average one, once a low-energy threshold was
245 crossed. This latter method is less computationally intensive.

246 The method described here is practically identical to the “Mean PMT pulse
247 model” used by Aykac *et al.* to analyse pulses from LSO crystals [21]. We
248 note that a procedure with a similar philosophy has been used for an entirely
249 different γ -ray spectroscopy application. The shapes of pulses recorded from
250 the segmented outer contacts of 36-fold AGATA Ge detectors are compared to
251 those found in a library of measured interactions [22]. This allows the interaction
252 position of γ rays to be found with a precision of a few mm in a large-volume
253 Ge detector.

254 3.5. ^{60}Co Source Results Summary and Comparison with Literature

255 A summary of the results obtained with each algorithm is shown in Table 1.
256 As ~ 1000 $\gamma - \gamma$ coincidences were analysed, then the statistical contribution to
257 the error ($\frac{\sigma}{\sqrt{n}}$) is around 2 ps. These results can be compared to the time reso-
258 lutions reported in the literature using analogue pulse-processing electronics. A
259 study of the performance of conical $\text{LaBr}_3(\text{Ce})$ detectors, with the same dimen-
260 sions as used here, reported a FWHM value of 110(3) ps with a ^{60}Co source [3].
261 The results obtained with the cubic polynomial slope fit are 30(1) % worse. In a

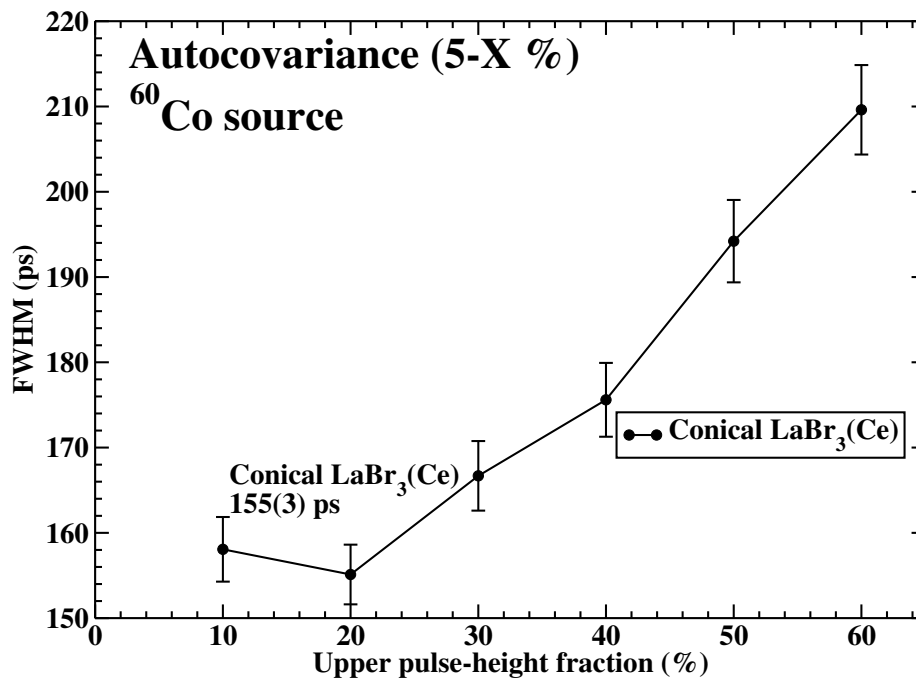


Figure 8: Full width half maximum (FWHM) of a digital autocovariance algorithm as a function of upper limit of the peak signal voltage for a single detector, de-convoluted from the measured distribution.

Leading Edge	Leading Edge Slope Fit	CFD	Autocovariance
177(4) ps	143(3) ps	178(4) ps	155(3) ps

Table 1: Summary of best values of FWHM achieved for each algorithm with a ^{60}Co source and a 10-bit 40 GS/s oscilloscope.

262 recent study using a 16-bit 5 GS/s digitizer with the same $\text{LaBr}_3(\text{Ce})$ detectors
 263 a time resolution of 106(1) ps was reported, using the same type of radioac-
 264 tive source and a timing algorithm developed using machine learning [10]. This
 265 result surpasses all the ones obtained in the present work. In [8] a spline inter-
 266 polation with a sinc function of the pulse rising slope using a 14-bit, 0.5 GS/s
 267 digitizer gave results equivalent to those reported using analogue electronics [3]
 268 for $1'' \times 1''$ $\text{LaBr}_3(\text{Ce})$ crystals [97 ps versus 98(2) ps]. This shows that a higher
 269 sampling frequency does not necessarily lead to improved time resolution if the
 270 vertical resolution is low and these points are discussed below.

271 4. Sampling Frequency

272 The performance of each algorithm was tested as a function of sampling fre-
 273 quency, using the data taken with the ^{60}Co source. The results are shown in
 274 Fig. 9. Optimal parameters at sampling rates of 40 GS/s, reported in previous
 275 sections were used throughout. Unsurprisingly the best performance is found
 276 at a sampling frequency of 40 GS/s, though little degradation of the FWHM
 277 is seen at 20 GS/s. At sampling frequencies of 4 or 5 GS/s, the resolution is
 278 typically 30–60 % worse. The results obtained in the present work differ from
 279 the conclusions of Aykac *et al.* [21] who studied the performance of small LSO
 280 detectors for PET applications. There they found that optimal digital algorithm
 281 performance was already attained at a sampling rate of 4 GS/s. Similarly War-
 282 burton and Henning [8] and Nakhostin *et al.* [10] were able to obtain results
 283 equivalent to the best ones achieved with analogue systems, though at lower
 284 frequencies of 0.5 and 4 GS/s using digitizers with 14 and 16 bits. This points
 285 towards vertical resolution being a more important parameter than sampling
 286 speed in the GS/s domain for $\text{LaBr}_3(\text{Ce})$ detectors. More formally the vertical

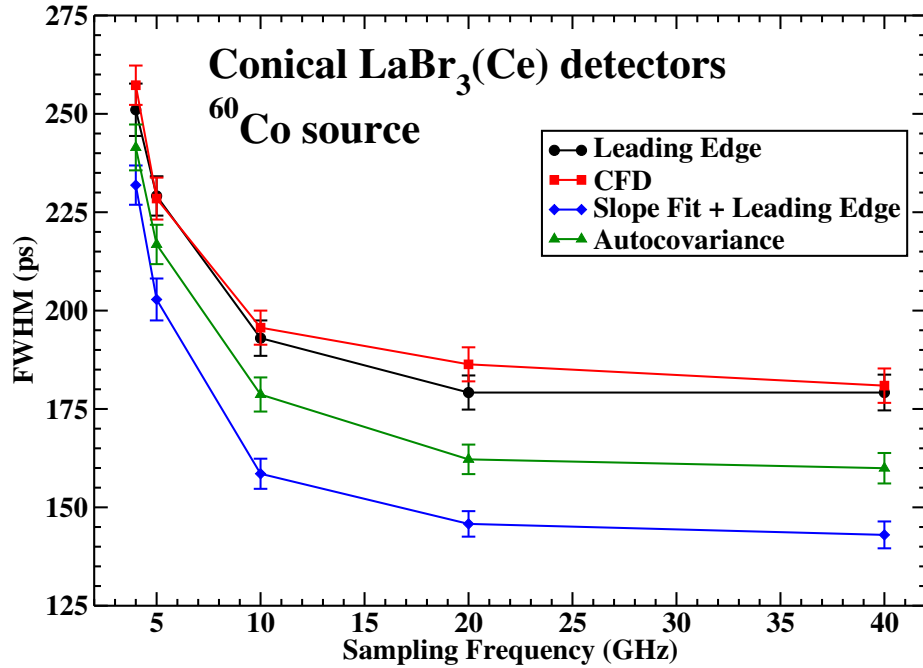


Figure 9: Full width half maxima (FWHM) of time peaks extracted with different digital algorithms as a function of sampling frequency for a single detector, de-convoluted from the measured distribution.

287 resolution (number of bits) must be high enough that the quantization error is
 288 below the electronic noise of the signal [18].

289 5. ^{152}Eu data

290 The evolution of the peak FWHM as a function of energy, measured with
 291 the ^{152}Eu source is shown in Fig. 10. Here one gate was set on the 344.3-keV
 292 γ -decay of ^{152}Gd and the peak FWHM was measured when the second gate was
 293 set at other photopeak energies (367.8, 411.1, 778.9, 1089.7 and 1299.1 keV).
 294 There were around 1000 counts in each coincidence time spectrum. The 344.3–
 295 1089.7-keV data points were removed from the fit as they were found to be
 296 systematically higher than the trend lines, likely due to contamination with the
 297 1085.9-keV transition in ^{152}Sm .

298 In Fig. 10 the autocovariance function is seen to have the best resolution
 299 across the range of energies studied. This energy range is typical of fast-timing

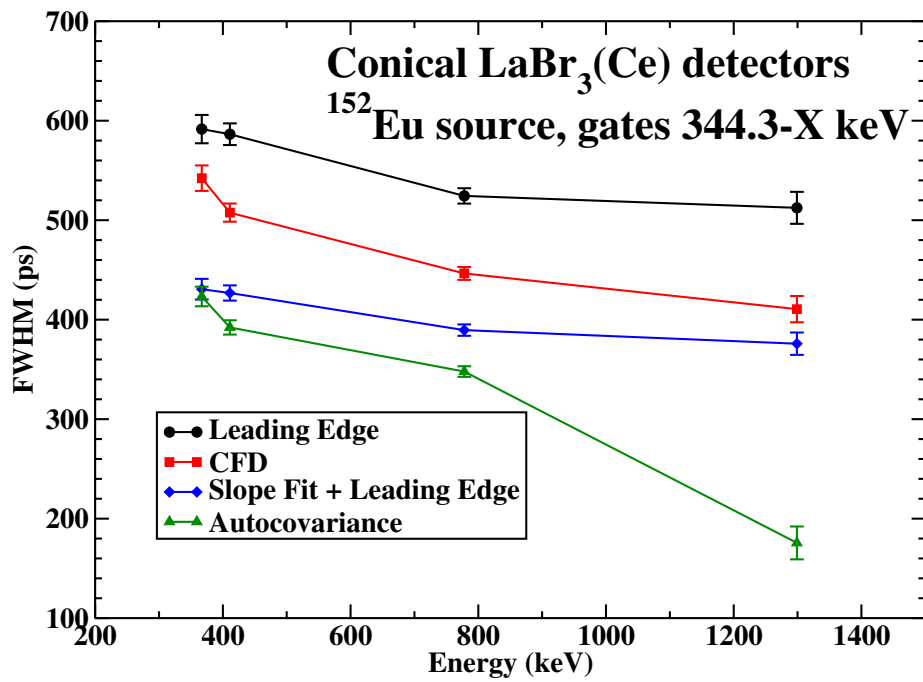


Figure 10: Measured peak full width half maximum (FWHM) values as a function of transitions found in coincidence with the 344.3-keV γ ray emitted following the decay of a ^{152}Eu source.

300 experiments aiming to study the lifetimes of excited states in the 10s-of-ps to
301 ns time range.

302 An important parameter in fast-timing measurements is the prompt-response
303 difference (PRD) [6, 7, 16]. This function is used to determine the zero-time
304 position as a function of energy and it depends on the settings of the analogue
305 discriminator used. The “walk” of this zero-time position typically changes
306 by a few hundred picoseconds over an energy range of 100 keV to 1.5 MeV.
307 Uncertainties in the PRD generally limit the precision of high-statistics fast-
308 timing measurements, hence the interest in obtaining PRD functions which are
309 as flat as possible [23, 24]. Despite the 3.1×10^6 coincident events recorded
310 with the ^{152}Eu source there were insufficient statistics to reliably determine the
311 PRDs of the all digital algorithms tested here.

312 **6. Conclusion**

313 The time resolutions obtained with four different timing algorithms have
314 been measured with a pair of 38-mm long, 38-mm wide truncated-cone shaped
315 $\text{LaBr}_3(\text{Ce})$ fast-timing detectors using a 10-bit, 40 GS/s oscilloscope. The time
316 resolution obtained with a cubic polynomial slope fit leading-edge algorithm
317 gave the best result with a ^{60}Co source [143(3) ps], though this is 30(1) % worse
318 than values achieved using analogue pulse-processing electronics. The perfor-
319 mance of the autocovariance function was slightly inferior [155(3) ps], but better
320 than the leading edge [177(4) ps] and constant-fraction [178(4) ps] algorithms.
321 The autocovariance function was found to have the best performance for coin-
322 cidences in the energy range 344.3–1299.1-keV. This may be because the cubic
323 polynomial slope fit algorithm used relies on a leading-edge threshold trigger,
324 with settings optimised for ^{60}Co lines. The performance of this algorithm may
325 therefore degrade when applied to lower-energy γ -rays. Reducing the sampling
326 frequency to 20 GS/s was found to only slightly degrade the time resolution of
327 these algorithms. The results obtained in the present work are a few tens-of-
328 picoseconds worse than those obtained using a 16-bit, 5 GS/s digitizer module

329 [106(1) ps] [10], demonstrating that high vertical resolution is more important
330 than sampling speed in the GS/s domain when using these detectors.

331 **7. Acknowledgments**

332 O. Bourrion, G. Bosson and Ch. Vescovi of the LPSC Grenoble are thanked
333 for helpful discussions. Financial support for this project was provided by
334 NuPNET/IN2P3. The IKP Cologne, NIPNE Bucharest and the ILL Greno-
335 ble are thanked for the loan of equipment. The authors (DD, MLGM, SM and
336 SC) acknowledge support from LabEx PRIMES (ANR-11-LABX-0063), INCa
337 Physique-Cancer (CLaRyS-UFT project) and the FP7 MEDINET-ENSAR2
338 framework.

339 **References**

- 340 [1] H. Mach, R. Gill, M. Moszyński, A method for picosecond lifetime mea-
341 surements for neutron-rich nuclei: (1) outline of the method, Nuclear In-
342 struments and Methods in Physics Research Section A 280 (1989) 49 – 72.
343 doi:[https://doi.org/10.1016/0168-9002\(89\)91272-2](https://doi.org/10.1016/0168-9002(89)91272-2).
- 344 [2] J. Krimmer, D. Dauvergne, J. Létang, E. Testa, Prompt-gamma
345 monitoring in hadrontherapy: A review, Nuclear Instruments
346 and Methods in Physics Research Section A 878 (2018) 58 – 73.
347 doi:<https://doi.org/10.1016/j.nima.2017.07.063>, radiation Imaging Tech-
348 niques and Applications.
- 349 [3] V. Vedia, M. Carmona-Gallardo, L. Fraile, H. Mach, J. Udías, Performance
350 evaluation of novel labr3(ce) scintillator geometries for fast-timing appli-
351 cations, Nuclear Instruments and Methods in Physics Research Section A
352 857 (2017) 98 – 105. doi:<https://doi.org/10.1016/j.nima.2017.03.030>.
- 353 [4] O. J. Roberts, A. M. Bruce, P. H. Regan, Z. Podolyk, C. M. Townsley, J. F.
354 Smith, K. F. Mulholland, A. Smith, A labr3: Ce fast-timing array for de-
355 spec at fair, Nuclear Instruments and Methods in Physics Research Section
356 A 748 (2014) 91 – 95. doi:<https://doi.org/10.1016/j.nima.2014.02.037>.

- 357 [5] L. Fraile, et al., Technical design report for the despec fast timing array,
358 2015.
- 359 [6] J.-M. Régis, H. Mach, G. Simpson, J. Jolie, G. Pascovici, N. Saed-
360 Samii, N. Warr, A. Bruce, J. Degenkolb, L. Fraile, C. Fransen,
361 D. Ghita, S. Kisyov, U. Koester, A. Korgul, S. Lalkovski, N. Marginean,
362 P. Mutti, B. Olaizola, Z. Podolyak, P. Regan, O. Roberts, M. Rudigier,
363 L. Stroe, W. Urban, D. Wilmsen, The generalized centroid differ-
364 ence method for picosecond sensitive determination of lifetimes of nu-
365 clear excited states using large fast-timing arrays, Nuclear Instruments
366 and Methods in Physics Research Section A 726 (2013) 191 – 202.
367 doi:<https://doi.org/10.1016/j.nima.2013.05.126>.
- 368 [7] J.-M. Régis, G. Simpson, A. Blanc, G. de France, M. Jentschel, U. Koester,
369 P. Mutti, V. Pazyi, N. Saed-Samii, T. Soldner, C. Ur, W. Urban, A. Bruce,
370 F. Drouet, L. Fraile, S. Ilieva, J. Jolie, W. Korten, T. Kroll, S. Lalkovski,
371 H. Mach, N. Marginean, G. Pascovici, Z. Podolyak, P. Regan, O. Roberts,
372 J. Smith, C. Townsley, A. Vancraeynest, N. Warr, Germanium-gated fast
373 timing of excited states in fission fragments using the exill & fatima spec-
374 trometer, Nuclear Instruments and Methods in Physics Research Section
375 A 763 (2014) 210 – 220. doi:<https://doi.org/10.1016/j.nima.2014.06.004>.
- 376 [8] W. K. Warburton, W. Hennig, New Algorithms for Improved Digital Pulse
377 Arrival Timing With Sub-GSps ADCs, IEEE Transactions on Nuclear
378 Science 64 (2017) 2938–2950. doi:[10.1109/TNS.2017.2766074](https://doi.org/10.1109/TNS.2017.2766074).
- 379 [9] M. Nakhostin, Z. Podolyak, P. H. Regan, Digital processing of signals
380 from labr3:ce scintillation detectors, Journal of Instrumentation 9 (2014)
381 C12049. URL: <http://stacks.iop.org/1748-0221/9/i=12/a=C12049>.
- 382 [10] V. Sánchez-Tembleque, V. Vedia, M. Carmona, L. M. Fraile, S. Ritt, J. M.
383 Udías, Digital strategies for time and energy measurement for ultra fast
384 scintillators, in: 2016 IEEE Nuclear Science Symposium, Medical Imag-

- 385 ing Conference and Room-Temperature Semiconductor Detector Workshop
386 (NSS/MIC/RTSD), 2016. doi:10.1109/NSSMIC.2016.8069677.
- 387 [11] F. Crespi, V. Vandone, S. Brambilla, F. Camera, B. Million, S. Riboldi,
388 O. Wieland, Hgpc detectors timing using pulse shape analysis techniques,
389 Nuclear Instruments and Methods in Physics Research Section A 620 (2010)
390 299 – 304. doi:<https://doi.org/10.1016/j.nima.2010.02.273>.
- 391 [12] M. Zeng, J. Cang, Z. Zeng, X. Yue, J. Cheng, Y. Liu, H. Ma, J. Li, Quanti-
392 tative analysis and efficiency study of psd methods for a labr3:ce detector,
393 Nuclear Instruments and Methods in Physics Research Section A 813 (2016)
394 56 – 61. doi:<https://doi.org/10.1016/j.nima.2015.12.045>.
- 395 [13] M. Aspinall, B. DMellow, R. Mackin, M. Joyce, Z. Jarrah, A. Pey-
396 ton, The empirical characterization of organic liquid scintillation detec-
397 tors by the normalized average of digitized pulse shapes, Nuclear Instru-
398 ments and Methods in Physics Research Section A 578 (2007) 261 – 266.
399 doi:<https://doi.org/10.1016/j.nima.2007.05.114>.
- 400 [14] P. Lecoq, Pushing the limits in time-of-flight pet imaging, IEEE Trans-
401 actions on Radiation and Plasma Medical Sciences 1 (2017) 473–485.
402 doi:10.1109/TRPMS.2017.2756674.
- 403 [15] J.-M. Régis, M. Rudigier, J. Jolie, A. Blazhev, C. Fransen, G. Pascovici,
404 N. Warr, The time-walk of analog constant fraction discriminators using
405 very fast scintillator detectors with linear and non-linear energy response,
406 Nuclear Instruments and Methods in Physics Research Section A 684 (2012)
407 36–45. doi:<http://dx.doi.org/10.1016/j.nima.2012.04.088>.
- 408 [16] J.-M. Régis, G. Pascovici, J. Jolie, M. Rudigier, The mirror symmetric
409 centroid difference method for picosecond lifetime measurements via co-
410 incidences using very fast labr3(ce) scintillator detectors, Nuclear Instru-
411 ments and Methods in Physics Research Section A 622 (2010) 83 – 92.
412 doi:<https://doi.org/10.1016/j.nima.2010.07.047>.

- 413 [17] M. Ahmed, B. Camanzi, J. Matheson, Characterisation of silicon
414 photomultipliers for time-of-flight pet, Nuclear Instruments and
415 Methods in Physics Research Section A 695 (2012) 252 – 256. URL:
416 <http://www.sciencedirect.com/science/article/pii/S0168900211022388>.
417 doi:<https://doi.org/10.1016/j.nima.2011.12.035>, new Developments in
418 Photodetection NDIP11.
- 419 [18] L. Bardelli, G. Poggi, M. Bini, G. Pasquali, N. Taccetti, Time measure-
420 ments by means of digital sampling techniques: a study case of 100ps fwhm
421 time resolution with a 100msample/s, 12bit digitizer, Nuclear Instruments
422 and Methods in Physics Research Section A 521 (2004) 480 – 492. URL:
423 <http://www.sciencedirect.com/science/article/pii/S0168900203030109>.
424 doi:<https://doi.org/10.1016/j.nima.2003.10.106>.
- 425 [19] A. Fallu-Labruyere, H. Tan, W. Hennig, W. Warburton, Time resolu-
426 tion studies using digital constant fraction discrimination, Nuclear In-
427 struments and Methods in Physics Research Section A 579 (2007) 247
428 – 251. doi:<https://doi.org/10.1016/j.nima.2007.04.048>, proceedings of the
429 11th Symposium on Radiation Measurements and Applications.
- 430 [20] R. F. Ling, Comparison of several algorithms for com-
431 puting sample means and variances, Journal of the
432 American Statistical Association 69 (1974) 859–866. URL:
433 <https://www.tandfonline.com/doi/abs/10.1080/01621459.1974.10480219>.
434 doi:[10.1080/01621459.1974.10480219](https://doi.org/10.1080/01621459.1974.10480219).
- 435 [21] M. Aykac, I. Hong, S. Cho, Timing performance comparison of dig-
436 ital methods in positron emission tomography, Nuclear Instruments
437 and Methods in Physics Research Section A 623 (2010) 1070 – 1081.
438 doi:<https://doi.org/10.1016/j.nima.2010.08.106>.
- 439 [22] S. Akkoyun, et al., Agata-advanced gamma tracking array, Nuclear In-
440 struments and Methods in Physics Research Section A 668 (2012) 26 – 58.
441 doi:<https://doi.org/10.1016/j.nima.2011.11.081>.

- 442 [23] J.-M. Régis, N. Saed-Samii, M. Rudigier, S. Ansari, M. Dannhoff,
443 A. Esmaylzadeh, C. Fransen, R.-B. Gerst, J. Jolie, V. Karay-
444 onchev, C. Mller-Gatermann, S. Stegemann, Reduced time walk
445 to below 50 ps using the multiplexed-start and multiplexed-stop
446 fast-timing technique with labr3(ce) detectors, Nuclear Instruments
447 and Methods in Physics Research Section A 823 (2016) 72 – 82.
448 doi:<https://doi.org/10.1016/j.nima.2016.04.010>.
- 449 [24] J.-M. Régis, M. Dannhoff, J. Jolie, A simple procedure for τ -lifetime
450 measurements using multi-element fast-timing arrays, Nuclear Instru-
451 ments and Methods in Physics Research Section A 897 (2018) 38 – 46.
452 doi:<https://doi.org/10.1016/j.nima.2018.04.047>.